

Physics of confinement improvement of plasmas with impurity injection in DIII-D

M. Murakami¹, G.R. McKee², G.L. Jackson, G.M. Staebler, D.A. Alexander³, D.R. Baker, G. Bateman⁴, L.R. Baylor¹, J.A. Boedo⁵, N.H. Brooks, K.H. Burrell, J.R. Cary^{3,6}, R.H. Cohen⁷, R.J. Colchin¹, J.C. DeBoo, E.J. Doyle⁸, D.R. Ernst⁹, T.E. Evans, C. Fenzi², C.M. Greenfield, D.E. Greenwood¹, R.J. Groebner, J.T. Hogan¹, W.A. Houlberg¹, A.W. Hyatt, R. Jayakumar⁷, T.C. Jernigan¹, R.A. Jong⁷, J.E. Kinsey⁴, A.H. Kritiz⁴, R.J. La Haye, L.L. Lao, C.J. Lasnier⁷, M.A. Makowski⁷, J. Mandrekas¹⁰, A.M. Messiaen¹¹, R.A. Moyer⁵, J. Ongena¹¹, A. Pankin⁴, T.W. Petrie, C.C. Petty, C.L. Rettig⁸, T.L. Rhodes⁸, B.W. Rice⁷, D.W. Ross¹², J.C. Rost¹³, S.G. Shasharina³, H.E. St. John, W.M. Stacey¹⁰, P.I. Strand¹, R.D. Sydora¹⁴, T.S. Taylor, D.M. Thomas, M.R. Wade¹, R.E. Waltz, W.P. West, K.L. Wong⁹, L. Zeng⁸, DIII-D Team
General Atomics,
San Diego, California, United States of America

Abstract. External impurity injection into L mode edge discharges in DIII-D has produced clear confinement improvement (a factor of 2 in energy confinement and neutron emission), reduction in all transport channels (particularly ion thermal diffusivity to the neoclassical level), and simultaneous reduction of long wavelength turbulence. Suppression of the long wavelength turbulence and transport reduction are attributed to synergistic effects of impurity induced enhancement of $\mathbf{E} \times \mathbf{B}$ shearing rate and reduction of toroidal drift wave turbulence growth rate. A prompt reduction of density fluctuations and local transport at the beginning of impurity injection appears to result from an increased gradient of toroidal rotation enhancing the $\mathbf{E} \times \mathbf{B}$ shearing. Transport simulations carried out using the National Transport Code Collaboration demonstration code with a gyro-Landau fluid model, GLF23, indicate that $\mathbf{E} \times \mathbf{B}$ shearing suppression is the dominant transport suppression mechanism.

1. Introduction

Optimizing energy and particle confinement in magnetically confined plasmas remains a central challenge to fusion energy research. Anomalous transport is believed to result primarily from temperature gradient and density gradient driven drift wave turbulence [1]. Therefore it is important to improve

the physics understanding of turbulence and transport and to enhance predictive capabilities through comparison of experiments, theory and simulation. A number of tokamak experiments, including ISX-B (Z mode) [2], TEXTOR-94 (RI mode) [3], TFTR [4], DIII-D [5, 6] and ASDEX-U [7], demonstrated that injection of controlled quantities of impurity into a plasma discharge can result in significant improvements of the global energy confinement. In the DIII-D

¹ Oak Ridge National Laboratory, Oak Ridge, Tennessee, United States of America.

² University of Wisconsin, Madison, Wisconsin, United States of America.

³ Tech-X Corporation, Boulder, Colorado, United States of America.

⁴ Lehigh University, Bethlehem, Pennsylvania, United States of America.

⁵ University of California, San Diego, California, United States of America.

⁶ University of Colorado, Boulder, Colorado, United States of America.

⁷ Lawrence Livermore National Laboratory, Livermore, California, United States of America.

⁸ University of California, Los Angeles, California, United States of America.

⁹ Princeton Plasma Physics Laboratory, Princeton University, Princeton, New Jersey, United States of America.

¹⁰ Georgia Institute of Technology, Atlanta, Georgia, United States of America.

¹¹ KMS/ERM, Brussels, Belgium.

¹² University of Texas, Austin, Texas, United States of America.

¹³ Massachusetts Institute of Technology, Cambridge, Massachusetts, United States of America.

¹⁴ University of Alberta, Edmonton, Alberta, Canada.

experiment, we have observed clear increases in confinement (from $H_{89P} \approx 1$ to $H_{89P} \leq 2$) and simultaneous reductions of long wavelength turbulence in L mode edge discharges which are directly correlated with external impurity injection. These observations provide an opportunity to test theory based understanding of mechanisms for confinement improvement. Reduction of ion thermal transport is attributed to impurity induced $\mathbf{E} \times \mathbf{B}$ shear suppression of turbulence fluctuations and reduction of toroidal drift wave turbulence growth rates. Impurity seeding can be used not only to produce a radiating mantle for reduction of heat fluxes to material surfaces, but also to control MHD stability by broadening pressure profiles in the reduced core transport region and/or the edge pedestal region.

2. DIII-D impurity injection experiments

Injection of noble gases (neon, argon and krypton) into L mode edge, negative central shear (sawtooth free) discharges in DIII-D has significantly improved the confinement [8, 9]. Compared with similar reference discharges without impurity injection, the confinement enhancement factor and neutron emission in neon injected discharges nearly doubled (Figs 1(a, b)). The ion and electron temperatures with neon injection exhibit increased central values (Figs 1(c, d)) as well as profile broadening. With neon injection, the electron density profile becomes more peaked owing to increased core values and decreased peaked edge values, resulting in the density peaking factor ($n_{e0}/\langle n_e \rangle$, ratio of central to volume average density) increasing from 1.2 to 1.5. The D_α radiation is reduced simultaneously with the change in the density profile, which is consistent with improvement of the particle confinement.

Simultaneously with confinement improvement, long wavelength density fluctuations are reduced. Density fluctuations, measured with beam emission spectroscopy (BES) [10] and far infrared (FIR) scattering [11], show that long wavelength turbulence ($k_\theta \rho_s \leq 0.6$, where ρ_s is the ion gyroradius evaluated at the sound speed) is dramatically reduced in the core ($\rho \leq 0.85$, where ρ is the square root of normalized toroidal flux). Temporally resolved BES measurements at $\rho = 0.7$, shown in Fig. 2, exhibit two distinct timescales in the turbulence suppression. A fast (within 10–20 ms) drop ($\sim 25\%$) in fluctuation amplitude immediately after the start of neon

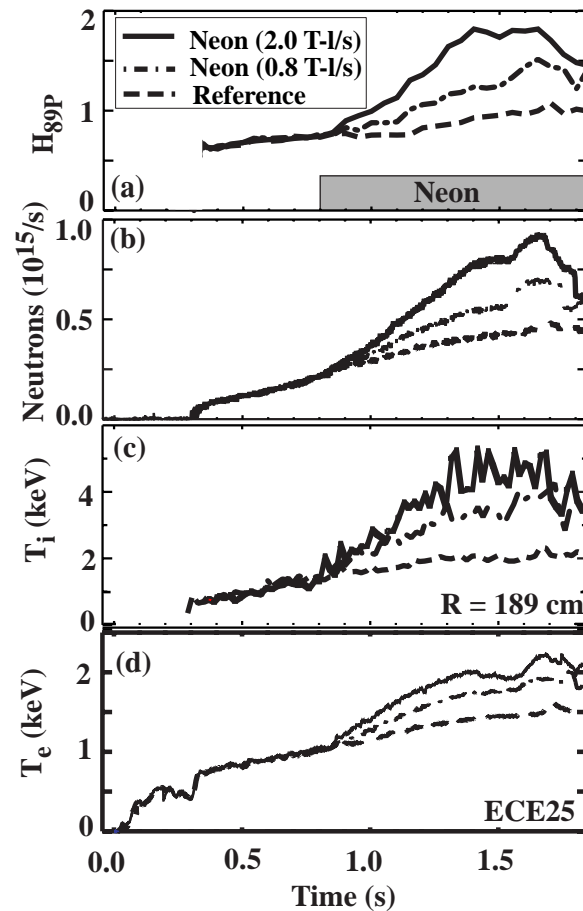


Figure 1. Characteristics of plasma parameters for discharges with a high (solid) and a medium (dot-dashed) quantity of neon and for a reference discharge without neon (dashed): (a) energy confinement enhancement factor, (b) neutrons, (c) central ion temperature, and (d) central electron temperature.

injection is followed by a slow reduction thereafter. The measurements also show that the large amplitude fluctuations near the edge ($0.85 \leq \rho \leq 1$) do not change significantly between the neon injected and the reference discharges. Langmuir probe measurements [12] show that turbulent particle flux is reduced at the edge, while the amplitude of the edge density fluctuations does not change significantly, which is consistent with BES and FIR scattering measurements.

Transport analysis shows that transport rates in all transport channels are reduced with neon injection. The analysis is carried out using the TRANSP profile analysis code [13] on the basis of the measured plasma profiles. The MHD equilibria have been reconstructed using the EFIT equilibrium code [14],

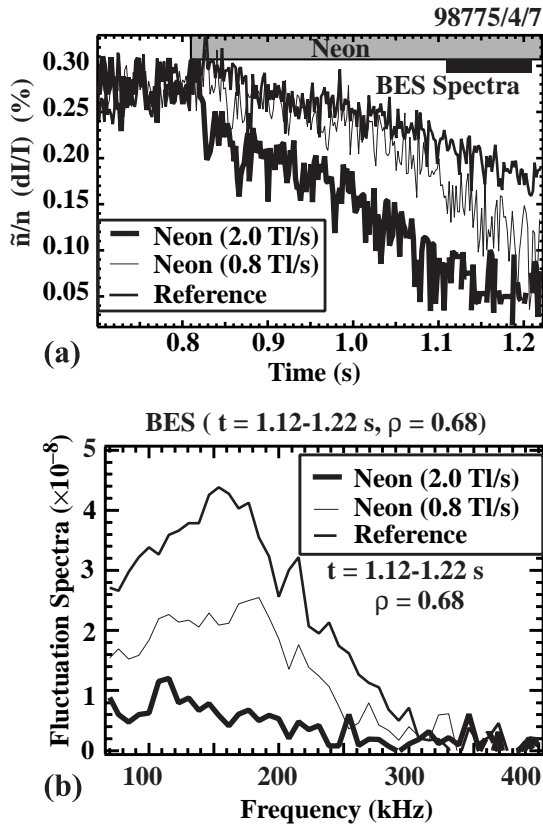


Figure 2. (a) Temporal evolution of density fluctuations measured with BES at $\rho = 0.7$, and (b) fluctuation spectra for different neon injection quantities.

including data from external magnetic field measurements and motional Stark effect field line pitch measurements, by taking into account the radial electric field [15], self-consistently including beam ion pressure as well as thermal electron and ion pressure. Profiles of effective charge (Z_{eff}) are determined from charge exchange recombination (CER) spectroscopy measurements of fully ionized carbon and neon impurities. The central Z_{eff} value increases from 1.5 (reference) to ≤ 3.4 (with neon), corresponding to a central neon density fraction (n_{Ne}/n_e) of up to 2.2%. On the other hand, intrinsic carbon density decreases by a factor of 2 upon neon injection. The modest dilution of the main fuel ions is compensated for by an increased central density, resulting in deuteron density remaining similar in both discharges. The factor of 2 increase in neutrons results primarily from an increase in the thermonuclear neutron rate arising from a higher ion temperature. Ion thermal diffusivity (χ_i) at $\rho = 0.66$ in the high quantity neon injection case quickly (within ~ 30 ms) decreases by a factor of 3, followed by a gradual reduction (Fig. 3(a)),

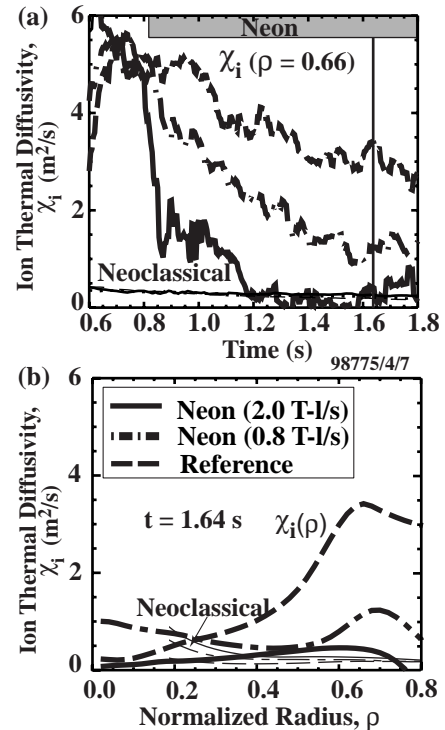


Figure 3. (a) Temporal evolution of ion thermal diffusivity at $r = 0.66$, and (b) ion thermal diffusivity profile at 1.64 s.

which is consistent with the BES measurement. The radial profile of χ_i at the peak performance time ($t = 1.64$ s) is given in Fig. 3(b), showing that χ_i is reduced throughout the profile to neoclassical levels (as calculated by the NCLASS model [16]). The electron thermal diffusivity (χ_e) shows a modest (≤ 1.5) reduction throughout the neon injection period. Both toroidal momentum diffusivity and particle diffusivity also decrease with neon injection. Therefore all transport channels are improved with neon injection.

3. Mechanisms for confinement improvement

The physical mechanisms that cause the observed reduction in turbulence and transport include impurity induced growth rate reduction of toroidal drift wave turbulence and increased radial electric field shear. The long wavelength turbulence observed in tokamak discharges is largely driven by ion temperature gradient (ITG) modes and trapped electron modes [17, 18]. Various studies have shown that impurities can affect the stability of these

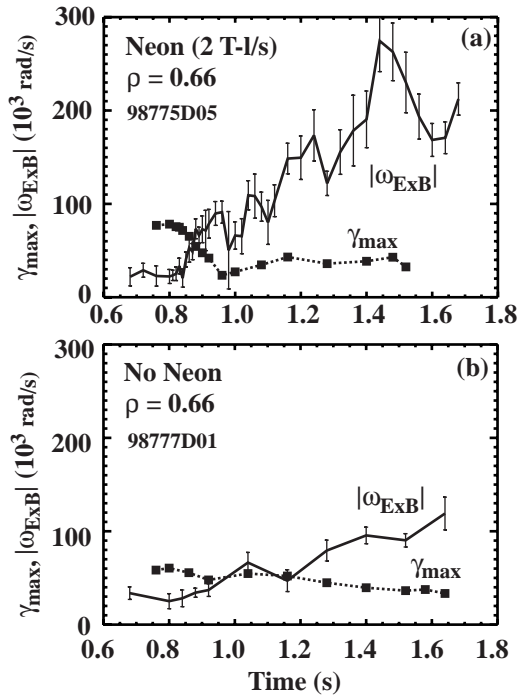


Figure 4. Time evolution of the $\mathbf{E} \times \mathbf{B}$ shearing rates (solid curves with error bars) and maximum linear growth rates (dashed curves) in (a) a neon injected and (b) a reference discharge.

microinstabilities, and that peaked impurity density profiles tend to stabilize ITG modes as a result of dilution of the main ions, direct mode stabilization by impurity ions and profile changes (e.g. caused by enhanced localized radiation). To explore such possibilities, the gyrokinetic stability (GKS) code [19] is used to calculate the linear growth rates at a given radial location and time using measured plasma profiles, including the full kinetic response of both ions and electrons in the actual magnetic geometry [20]. In addition, $\mathbf{E} \times \mathbf{B}$ shear affects stabilization of microturbulence by eddy shearing and non-linear turbulence decorrelation [21, 22]. It has been predicted theoretically and demonstrated experimentally that long wavelength fluctuations are suppressed in plasmas when the local $\mathbf{E} \times \mathbf{B}$ shearing rate [23]

$$\omega_{\mathbf{E} \times \mathbf{B}} = [(RB_\theta)^2/B](\partial/\partial\psi)[E_r/(RB_\theta)] \quad (1)$$

exceeds the linear growth rate of the most unstable modes. The $\mathbf{E} \times \mathbf{B}$ shearing rates were determined from the radial force balance of the intrinsic carbon ions based on CER measurements of toroidal and poloidal rotation and the pressure gradient along the outer midplane.

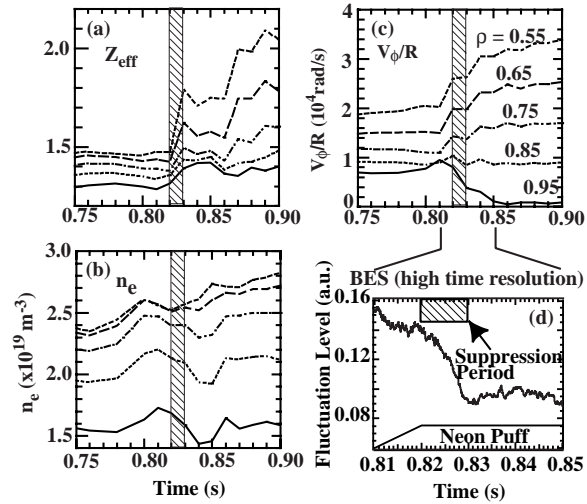


Figure 5. Changes of profiles in (a) Z_{eff} , (b) electron density, and (c) angular toroidal rotation frequency around the start of neon injection when (d) BES fluctuation amplitude drops by $\sim 25\%$, on the basis of BES wavelet analysis.

In discharges with neon injection, the $\mathbf{E} \times \mathbf{B}$ shearing rate significantly exceeds the linear growth rate of turbulence. Figure 4 shows the temporal evolution of the $\mathbf{E} \times \mathbf{B}$ shearing and the maximum linear growth rates for the neon injected and reference shots at $\rho = 0.66$. Overall, the $\mathbf{E} \times \mathbf{B}$ shearing rates with neon injection are a factor of 2 larger than those in the reference shot without neon. At the same time, the maximum growth rates are lower with neon injection.

The prompt density fluctuation drop (~ 10 ms) at the beginning of neon injection suggests a cause for the confinement improvement. Figure 5 shows the profile changes in Z_{eff} , electron density and angular toroidal rotation frequency near the start of impurity injection (no smoothing is applied to the data). The rise in Ne^{10+} density occurs within 10 ms (0.81–0.82 s). There is some peaking of the electron density profile, as is commonly observed with impurity injection [24]. However, the effect on the reduction of the maximum growth rate (as shown in Fig. 5(a)) is rather modest. In contrast, the toroidal rotation profile changes rapidly (in less than 20 ms, the time resolution of the CER rotation measurement); rotation decreases for $\rho > 0.85$ and increases for $\rho < 0.85$. Further simulation and analysis are required to determine the interplay between the rapid neon influx, toroidal rotation gradient increase and observed turbulence reduction. The local transport

reduction and suppression of low k turbulence (Fig. 5(d)) appear to result from an increasing rotation gradient enhancing the $\mathbf{E} \times \mathbf{B}$ shear.

The electron thermal diffusivity also decreases with neon injection. The density profile peaking factor increases, and the parameter $\eta_e = L_{ne}/L_{Te}$, important in the electron temperature gradient mode, decreases. Preliminary analysis of short wavelength fluctuations measured with FIR scattering ($k_\theta = 13 \text{ cm}^{-1}$) shows that the RMS amplitude decreases in a bursting fashion during impurity injection. The average fluctuation level is correlated well with electron thermal diffusivity as impurity quantities and species are varied. Unfortunately, uncertainties in the source of these fluctuations exist because the expected large $\mathbf{E} \times \mathbf{B}$ Doppler shift is not evident in the fluctuation spectra.

4. Theory based transport modelling

The gyro-Landau fluid model GLF23 [25] is used to increase understanding of the relative roles of individual confinement improvement mechanisms. GLF23 is a 1-D dispersion type drift wave model developed from the approximate linear growth rates from the GKS code and uses parameterized results from non-linear gyro-Landau fluid simulations to determine the saturation levels. This critical gradient drift ballooning mode based model yields quasi-linear estimates of transport coefficients for the electron and ion temperatures, hydrogenic particle and impurity densities, and toroidal momentum. The model includes $\mathbf{E} \times \mathbf{B}$ flow shear as well as other turbulence suppression mechanisms. The flux quantity of the $\mathbf{E} \times \mathbf{B}$ shearing rate [26] is computed using the Doppler shift shearing rate extended to real geometry

$$\gamma_{\mathbf{E} \times \mathbf{B}} = (r/q)\partial/\partial r[E_r/(RB_\theta)] \quad (2)$$

where r is the midplane minor radius. Compared with the shearing rate (Eq. (1)) based on the two point decorrelation analysis on the outer midplane, $\gamma_{\mathbf{E} \times \mathbf{B}}$ is a factor of 2–4 lower under the present experimental conditions. The net turbulence transport is calculated from

$$\gamma_{net} = \gamma_{max} - \alpha_E |\gamma_{\mathbf{E} \times \mathbf{B}}| \quad (3)$$

where α_E is a constant for $\mathbf{E} \times \mathbf{B}$ shear stabilization.

Time dependent simulations were carried out using the National Transport Code Collaboration (NTCC) demonstration code [27]. This code used the DIII-D neon shots as the primary test case for the code development. In these simulations, both electron and ion thermal transport were evolved self-consistently with inputs of time dependent experimental electron and impurity density and toroidal momentum profiles. Experimental boundary conditions were used at a normalized radius of $\rho = 0.9$. The simulations were carried out taking time dependent sources, sinks and equilibria provided by the TRANSP code. Figure 6 shows T_i and T_e profiles at the final simulation time, 1.58 s, for the neon injected shot, and time histories of T_i and T_e at $\rho = 0, 0.33$ and 0.66 . The T_i simulation agrees well with the experiment, while T_e is somewhat overestimated in the simulation. While $\gamma_{\mathbf{E} \times \mathbf{B}} > \gamma_{max}$ eliminates transport from low k drift ballooning modes, the electron thermal transport remains anomalous owing to a remaining presence of high k electron temperature gradient modes for which $\mathbf{E} \times \mathbf{B}$ shearing is ineffective.

The importance of $\mathbf{E} \times \mathbf{B}$ flow shear is illustrated by the simulation of the neon injected shot with three different $\mathbf{E} \times \mathbf{B}$ flow shear rates — experimental $\gamma_{\mathbf{E} \times \mathbf{B}}$, the rate from the reference shot without neon and the rate with no $\mathbf{E} \times \mathbf{B}$ shear at all ($\alpha_E = 0$), as shown in Fig. 7. The $\gamma_{\mathbf{E} \times \mathbf{B}}$ values in the above simulations have used experimentally measured poloidal rotation velocity (V_{pol}). When $\gamma_{\mathbf{E} \times \mathbf{B}}$ is based on neoclassically calculated V_{pol} , as is customarily done [28, 29], we find that the best agreement with the experiment is with $\alpha_E = 1$.

The role of the neon impurity is demonstrated in simulations with conditions of the neon injected shot but with Z_{eff} and electron density profiles from the reference shot without neon. The simulation was started from the time at which neon has already established the improved state ($t = 1.2$ s) but switched to the no-neon condition ($Z_{eff} = 1.4$ and broad density profile) while maintaining the shearing rate. The ion temperature after 0.38 s (about 3 confinement times) is still elevated. This result suggests an experimental scenario where neon injection is used as a trigger and is switched off after confinement improvement is achieved. This scenario will be explored in future experiments. Recently magnetic braking was used in an experiment to directly test the role of $\mathbf{E} \times \mathbf{B}$ shearing in improved confinement with neon injection [30].

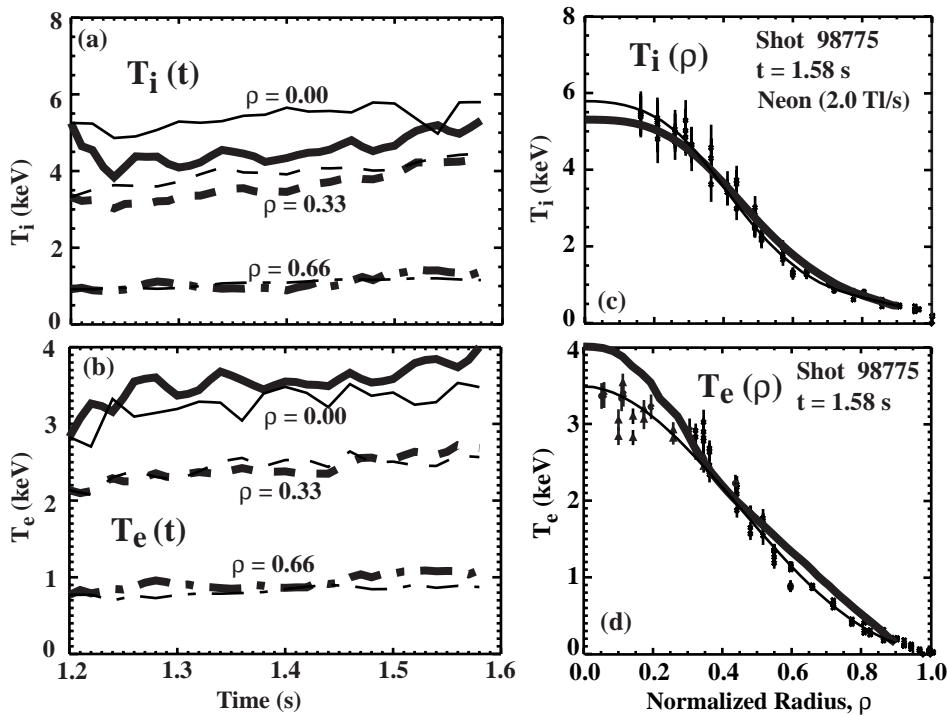


Figure 6. Comparison of GLF23 transport simulation results (bold lines) with the experiments (fine lines) for the neon injected shot (98775): temporal evolution of (a) ion and (b) electron temperature at $\rho = 0, 0.33$ and 0.66 ; (c) ion and (d) electron temperature profiles at the final simulation time (1.58 s).

5. Summary

External impurity injection into L mode edge discharges in DIII-D has produced clear increases in confinement (with a factor of 2 increase in energy confinement and neutron emission), reduction in all transport channels (particularly χ_i to the neoclassical level) and a simultaneous reduction of long wavelength turbulence. Gyrokinetic analysis showed that suppression of long wavelength turbulence and reduction of ion thermal transport are attributable to impurity driven enhancement of the $\mathbf{E} \times \mathbf{B}$ shearing rate and a reduction of toroidal drift wave turbulence. The transport reduction appears to result from a positive feedback synergism between growth rate reduction, $\mathbf{E} \times \mathbf{B}$ shear increase and inward particle and/or momentum convection associated with the neon influx. GLF23 transport simulations show that $\mathbf{E} \times \mathbf{B}$ shearing suppression plays the dominant role by suppression of transport. These results suggest that impurity seeding can achieve good energy and particle confinement while maintaining a highly radiative, cool L mode edge with low heat flux to first material surfaces.

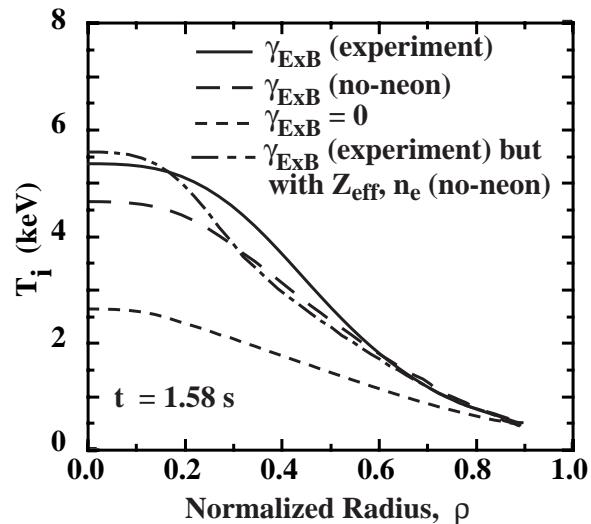


Figure 7. Sensitivities of predicted ion temperature profiles against varying $\mathbf{E} \times \mathbf{B}$ shearing rates and against replacing electron density and Z_{eff} profiles with those from the reference shot without neon injection. Simulations were carried out from 1.20 to 1.58 s.

Acknowledgements

This is a report of work supported by the US Department of Energy (DOE) under contracts DE-AC03-99ER54463, DE-AC05-00OR22725, W-7405-ENG-48 and DE-AC02-76CH03073, and grants DE-FG02-92ER54139, DE-FG02-92ER54141, DE-FG03-95ER54294, DE-FG03-86ER53225 and DE-FG02-94ER54235 APTE. The National Transport Code collaboration project is supported by contracts and grants provided by the US DOE.

References

- [1] Carreras, B.A., IEEE Trans. Plasma Sci. **25** (1997) 1281.
- [2] Lazarus, E.A., et al., J. Nucl. Mater. **121** (1984) 61.
- [3] Messiaen, A.M., et al., Phys. Rev. Lett. **77** (1996) 2487.
- [4] Hill, K., et al., Phys. Plasmas **6** (1999) 877.
- [5] McKee, G.R., et al., Phys. Rev. Lett. **84** (2000) 1922.
- [6] Jackson, G.L., et al., J. Nucl. Mater. **266–269** (1999) 380.
- [7] Gruber, O., et al., Phys. Rev. Lett. **74** (1995) 4217.
- [8] McKee, G.R., et al., Phys. Plasmas **7** (2000) 1870.
- [9] Murakami, M., et al., in Controlled Fusion and Plasma Physics (Proc. 27th Eur. Conf. Budapest, 2000), Vol. 24, European Physical Society, Geneva (2000) paper P2.026.
- [10] McKee, G.R., et al., Rev. Sci. Instrum. **70** (1999) 913.
- [11] Rettig, C.C., et al., Rev. Sci. Instrum. **61** (1990) 3010.
- [12] Moyer, R.A., et al., Phys. Plasmas **2** (1995) 2397.
- [13] Hawryluk, R.J., et al., in Physics of Plasmas Close to Thermonuclear Conditions (Proc. Course Varenna, 1979), Vol. 1, CEC, Brussels (1979) 19.
- [14] Lao, L.L., et al., Nucl. Fusion **30** (1990) 1035.
- [15] Rice, B.W., Burrell, K.H., Lao, L.L., Nucl. Fusion **37** (1997) 517.
- [16] Houlberg, W.A., Shaing, K.C., Hirshman, S.P., Zarnstorff, M.C., Phys. Plasmas **4** (1997) 3230.
- [17] Horton, W., Rev. Mod. Phys. **71** (1999) 735, and references therein.
- [18] Sydora, R.D., et al., IAEA-CN-77/THP1/27, paper presented at 18th IAEA Conf. on Fusion Energy, Sorrento, 2000.
- [19] Kotschenreuther, M., et al., Comput. Phys. Commun. **88** (1995) 128.
- [20] Miller, R.L., Phys. Plasmas **5** (1998) 973.
- [21] Burrell, K.H., Phys. Plasmas **4** (1997) 1499, and references therein.
- [22] Waltz, R.E., Dewar, R.L., Garbet, X., Phys. Plasmas **5** (1998) 1784.
- [23] Hahm, T.S., Burrell, K.H., Phys. Plasmas **2** (1995) 1648.
- [24] Tokar, M.Z., et al., Phys. Rev. Lett. **84** (2000) 895.
- [25] Waltz, R.E., et al., Phys. Plasmas **4** (1997) 2482.
- [26] Waltz, R.E., Miller, R.L., Phys. Plasmas **6** (1999) 4265.
- [27] NTCC Team, “The US National Transport Code Collaboration”, Proc. 17th Int. Conf. on Numerical Simulation of Plasmas, Banff, 2000, pp. 172–175.
- [28] Kinsey, J.E., et al., in Controlled Fusion and Plasma Physics (Proc. 26th Eur. Conf. Maastricht, 1999), Vol. 23J, European Physical Society, Geneva (1999) 1205.
- [29] Ernst, D., et al., Phys. Rev. Lett. **81** (1998) 2454.
- [30] Ernst, D., et al., Bull. Am. Phys. Soc. **45** (2000) 221.

(Manuscript received 4 October 2000

Final manuscript accepted 24 November 2000)

E-mail address of M. Murakami:

murakami@fusion.gat.com

Subject classification: F2, Tm; J1, Te; C0, Te